

Experimental and numerical study of the performance of Ultra High Performance Fiber Reinforced Concrete for the flexural strengthening of full scale Reinforced Concrete members

Spyridon A. Paschalis¹, Andreas P. Lampropoulos², Ourania Tsioulou²

¹School of Engineering, University of Bolton, Calderwood Building, Deane Road, Bolton, BL3 5AB, UK

²School of Environment and Technology, University of Brighton, Cockcroft building, Lewes Road, Brighton, BN2 4GJ, UK

Abstract

Ultra High Performance Fiber Reinforced Concrete (UHPFRC) is a cementitious material with enhanced mechanical characteristics. The superior mechanical properties of UHPFRC compared to conventional concrete, as well as the ease of preparation and application, make the use of this material attractive for strengthening applications. In the present study, an extensive experimental investigation on full scale Reinforced Concrete (RC) beams strengthened with UHPFRC layers has been conducted. Additional UHPFRC layers with and without steel bars have been added to the RC beams and the efficiency of the examined technique has been examined through flexural tests. An additional investigation has been conducted on the interface characteristics between UHPFRC and concrete through push-off tests. Finally, finite element analysis has been conducted and crucial parameters of the examined technique have been investigated. The results of the present study indicated that the strengthening with UHPFRC layers is a well promising technique, as in all the examined cases the performance of the strengthened elements was improved. Also, a good interface connection between UHPFRC and concrete was identified, with low measurements of slips at the interface.

Keywords

UHPFRC; Full Scale; Strengthening; UHPFRC to Concrete Interfaces; Push-off tests, Finite Element Analysis

1. Introduction

Most of the new Reinforced Concrete (RC) structures which are built nowadays meet the criteria for safe building design. Nevertheless, we cannot claim the same for structures built in the past. These old structures make up the majority of the total number of existing structures today. The majority of these structures have been designed either without any regulations, or based on old code provisions which have been proved to be structurally deficient. Consequently, the loading carrying capacity system of these structures need to be upgraded. The present research is focused on the strengthening of RC elements using UHPFRC layers.

To date, there are several published studies on the mechanical properties of UHPFRC. Kang et al. [1] and Yoo et al. [2] examined the effect of fiber content on the flexural strength of UHPFRC, and it was found that both the flexural strength and the structural ductility increased at increasingly fiber content. The effect fiber content on the tensile characteristics of UHPFRC was investigated by Paschalis and Lampropoulos [3] and for the different fiber contents, different stress-strain models were proposed. Also, in this study, the effect of curing regime on the tensile characteristics of UHPFRC was investigated and the optimum curing period was proposed. Neocleous et al. [4], used an inverse finite element analysis method to derive the tensile characteristics of Steel Fiber Reinforced Concrete (SFRC), while Nicolaidis et al. [5] developed an optimum mixture for Ultra High Performance Cementitious Composites using components available in Cyprus. The fiber distribution is an important parameter affecting the performance of UHPFRC and this was highlighted by Ferrara et al. [6]. The study of the performance of UHPFRC in earthquake prone areas is of high importance. Paschalis and

Lampropoulos [7] investigated the response of UHPFRC under cyclic loading for different fiber contents, and a constitutive model which can predict the hysteretic characteristics of UHPFRC under cyclic loading was proposed. The unique properties of UHPFRC have also been extensively investigated in numerous previous studies [8-14].

The use of UHPFRC for repair and strengthening applications has been investigated in a limited number of experimental, analytical and numerical studies. Habel et al. [15] conducted an extensive analytical investigation on the performance of composite UHPFRC-concrete elements under the assumption of perfect bond between the old and the new element where the efficiency of this technique was highlighted. Numerical study has been presented by Lampropoulos et al. [16] where the structural performance of beams strengthened with UHPFRC layers has been studied through Finite Element Analysis and comparisons with conventional methods have also been presented. Bruhwiler and Denarie [17] presented a realistic application of the UHPFRC for the rehabilitation of RC structures, such as a road bridge, a bridge pier and an industrial floor, and the benefits of the application of UHPFRC for the rehabilitation of concrete structures were highlighted. Safdar et al. [18], investigated the application of UHPFRC as a repair material and the flexural response of composite UHPFRC-RC elements was examined. The experimental results indicated that the use of UHPFRC layers increased the stiffness and the resistance of the elements. Talayeh and Bruhwiler [19] investigated the performance of reinforced UHPFRC beams subjected to bending and shear in a cantilever beam setup and they found that most of the specimens failed due to a flexural failure at a force of 2 to 2.8 higher than the resistance of the control specimens.

The flexural strengthening of RC members using RC layers is a popular and reliable technique. The use of the UHPFRC for the same purposes is a well promising technique which can increase the performance of the technique. However, further research on this topic is consider necessary in order to investigate all these crucial parameters concern the examined technique.

According to Tsioulou et al. [20], in case of RC elements strengthened with additional concrete layers, one of the most crucial parameters is the behaviour of the interface between the old and the new concrete since inadequate bonding may lead to premature failure of the strengthened elements. The behavior of the interface between the existing RC elements and the new UHPFRC layers is a crucial topic which has not been studied to date and needs investigation. The present study aims to investigate in depth the performance of UHPFRC for the strengthening of existing RC members and to provide useful information to both the scientific community and practitioners through an extensive experimental and numerical investigation. Crucial parameters which have never been investigated before, such as the interface characteristics between UHPFRC and concrete, the effect of layer depth and steel ratio on the performance of the examined technique, are investigated in the present study. Also, in the present study, suggestions for the application of the examined technique in real practice are presented.

The experimental part of the present study is focused on the flexural strengthening of RC beams using different strengthening configurations. More specifically, the performance of full scale RC beams strengthened with additional UHPFRC layers was investigated. UHPFRC layers with and without steel bars were cast to the tensile side of beams and the specimens were tested under 4 point flexural loading. During the testing, measurements of the slip at the interface between the UHPFRC layer and the existing RC beams were recorded and the results were compared with available data in the literature for concrete to concrete interfaces. Additionally, push-off tests were conducted in order to evaluate the characteristics of conventional concrete to UHPFRC interfaces. Finally, finite element analysis was conducted and crucial parameters of the examined technique were investigated numerically.

2. Experimental program

2.1 Experimental program for the strengthening of existing RC beams and the push-off tests

In the present study, six identical full scale RC beams were constructed and used for evaluation of the performance of RC beams strengthened with UHPFRC layers. Two RC beams were used as control beams for the evaluation of the performance of existing beams prior to strengthening, while four beams were strengthened with layers at the tensile side. In case of the strengthened beams, the additional UHPFRC layers were applied two months after the casting of the initial beams and the strengthened beams were tested over four months. For this investigation, two beams were strengthened with UHPFRC layers and two beams were strengthened with UHPFRC layers and steel bars (Table 1).

The geometry and the reinforcement of the initial beams are presented in Figure 1. As shown in this figure, the existing RC beams were reinforced at the tensile side with two longitudinal ribbed steel bars with a diameter of 12 and a length of 2150 mm. On the contrary, the reinforcement at the compressive side of beams was used to support the stirrups. In order to avoid shear failure of the beams, shear reinforcement, according to Eurocode 2 [21] was placed along the whole length of the beams. More specifically, stirrups with a diameter of 10 mm and a spacing of 150 mm were placed as shear reinforcement. Plastic spacers were used in order to ensure the required concrete cover of 25 mm of the reinforcement. The constructed UHPFRC layers had a depth of 50 mm, a breadth of 150 mm and were cast along the whole length of the tensile side of the beams (Figure 2). Two ribbed steel bars with a diameter of 10 mm, a length of 2150 mm and a concrete cover of 25 mm were used as a reinforcement of the UHPFRC layers. All the steel bars of the present investigation were grade B 500C.

Finally, for the push-off tests two concrete cubes with side length of 100 mm were prepared first and placed in the molds, and later on, the UHPFRC cube was cast. The geometry of the specimens is presented in Figure 3. The specimens were tested two months after casting.

2.2 Preparation of the materials

For the preparation of the examined beams, the reinforcement was assembled first, and then the reinforcement was placed in the moulds. Once the reinforcement was ready, the concrete was poured in the moulds. The concrete mixture design used for the initial beams is presented in Table 2. All the initial beams were wet cured daily for 28 days, while after this period the beams were wet cured every two days and until the casting of the layers. For the preparation of the UHPFRC, silica sand with a maximum particle size of 500 μ m was used together with silica fume, Ground Granulated Blast Furnace Slag (GGBS) and cement class 52.5 R type I. Low water/cement ratio of 0.28 was also used together with polycarboxylate superplasticizer. A percentage of 3% per volume steel fibers was used for the preparation of the UHPFRC mixture. In this investigation straight steel fibers with a length of 13 mm, a diameter of 0.16 mm, and a tensile strength of 3000 MPa were used, while the modulus of elasticity was 200 GPa. The examined mixture design is presented in Table 3.

Before the casting of the layers the surface of the RC beams was roughened to a depth of 2-2.5 mm, which according to fib bulletin 55 [22] can be classified as rough interface. For the preparation of the surface, a pistol grip needle scaler was employed (Figure 4), and the sand patch method was used to quantify the concrete surface texture. Before the casting of the layers, the surface was cleaned carefully using high pressure water. Then, the additional layers were cast (Figures 5a-5c) and after the demoulding, two days casting, the specimens were wet cured daily for 28 days. After this period the beams were wet cured every two days and until the testing of the strengthened beams.

Finally, for the roughening of the cubes' surface , for the push-off tests, a pistol grip needle scaler was used following exactly the same procedure which was used for the interface preparation of the interface of the full scale beams. The roughness depth was equal to 2-2.5 mm, similar to the one of the full scale beams.

In the present study the layer was cast upside down. This procedure is different compared to the procedure which is followed in real practice. One parameter which could be affected, is the distribution of the fibers in the layers. However, this is not expected to affect the experimental results. Based on Paschalis and Lampropoulos [13] the fiber distribution and the overall performance of the UHPFRC layers is not significantly affected in small layer depths, like the layer depths investigated in the present study.

The first step for the application of the technique in real practice is to roughen the interface between the new layer and the existing beam until the aggregates are exposed. In cases of damaged beams in bending, the existing reinforcement should be exposed and the new reinforcement must be connected to the old one [23]. This can be achieved using connection bars between the existing and the new bars as presented in Figure 6.

An important parameter for the application of the technique in real practice is the casting of the layers. The new layers can be cast, either by spraying as shotcrete or in-situ with the appropriate arrangement of the formwork. Shotcrete is commonly used for the casting of concrete layers and jackets and the same procedure can be followed for the UHPFRC layers. There are studies which have investigated the application of UHPFRC as shotcrete [24] and this technique has been successfully applied in real practice [25], [26]. Also, the casting of the layers can take place in-situ with the appropriate arrangement of the formwork. UHPFRC is a material with excellent rheological properties [3], similar to self-compacting concrete. The construction of existing concrete layers, is also described in detail by the Technical Chamber of Greece [23] and similar procedure can be followed for UHPFRC.

2.3 The properties of the materials

For the evaluation of the compressive strength of concrete, standard cube specimens with side length of 100 mm were prepared from the same mixture used for the preparation of the existing RC beams. The tests were performed under a loading rate of 0.6 MPa/s, according to BS EN 12390-3:2009 [27]. The average compressive strength of three concrete cubes was found to be equal to 30.9 MPa and the standard deviation was 2.34 MPa.

For the investigation of the properties of the UHPFRC layers, dog bone shaped and cube specimens were prepared from the same mixture used for the construction of the layers. The specimens were wet-cured daily for twenty-eight days and tested in the same time frame with the layers, namely two months after casting. For the direct tensile tests a displacement rate of 7 $\mu\text{m/s}$ was adopted. The experimental setup together with the dimensions of the specimens are presented in Figures 7a and 7b. As illustrated in Figure 7b, the extension of the specimens was recorded using a Linear Variable Differential Transformer (LVDT) connected to a special steel frame. This setup was used in order to measure directly the average of the extensions on both sides of the specimens. As can be seen in the same figure, the specimens failed due a single crack which was localized in the middle of the length of the specimens. The tensile stress-strain results are illustrated in Figure 8.

The average maximum stress was found to be equal to 11.5 MPa and the standard deviation was equal to 1.26 MPa. From the linear part of the stress-strain curve the modulus of elasticity was calculated equal to 51 GPa. For the investigation of the compressive strength of the examined UHPFRC mixture, three standard cubes were prepared and tested in the same time frame (two months) and the average compressive strength was found to be equal to 136.5 MPa and the standard deviation was 5.5 MPa.

Finally, according to BS 4449:2005 [28], the yield stress of steel bars B 500 C is equal to 500 MPa, while the ratio of the maximum tensile stress to the yield stress, is in the range of 1.15-1.3. The elongation at the maximum load is equal to 7.5%.

2.4 The testing of the specimens

For the testing of the examined beams, a four point loading test under a constant displacement rate of 8 $\mu\text{m/s}$ was conducted, which is in agreement with the loading rate used by Tsioulou et al. [20], leading to comparable results. The experimental setup for these tests is presented in Figure 9. As can be seen in Figure 9 two roller supports were used for the testing of the beam. During the testing, the load was recorded alongside with the deflection at the middle of the span length and both sides of the beam. As shown in Figure 9, the deflection was measured using Linear Variable Differential Transformers (LVDTs) with an accuracy of 1 μm . For the beams strengthened with layers, the slip at the interface was also measured using nine LVDTs, in total, which were placed on both sides. The position of the LVDTs is presented in Figures 10a and 10b. As can be seen in Figure 10a, the LVDTs on side 1 were placed symmetrically between the supports and the two loading points, while on side 2 (Figure 10b) 3 more LVDTs were used. The LVDTs on side 2 were used for the validation of the results obtained on side 1. As can be seen in Figures 10a and 10b, LVDTs 7 and 9 were placed in the same position with LVDTs 5 and 1 respectively, but at the opposite side. On the contrary the LVDT 8 was placed in between the two loading points. The recordings of each one of these LVDTs during the testing are presented in the following sections. As shown in Figure 10c, the LVDTs were attached on the RC beam using metal angle sections, which were glued on the existing RC beams and the layers.

In Figure 11, the experimental setup for the push off tests is presented. During the testing, a constant stress equal to 1 MPa was applied to the specimens through a hydraulic jack. As can

be seen in Figures 3 and 11, a load cell in contact with the specimens was also used to record the load and to secure a constant value during the testing. At the same time, a vertical load was also applied to the UHPFRC cube through an actuator under a constant displacement control of 1 $\mu\text{m/s}$. Finally, two LVDTs were placed on each side of the specimens for the measurement of slip at the interface.

2.5 The experimental results from the full scale testing

The experimental results for the load and the deflection of the control beams, the beams strengthened with UHPFRC layers and the beams strengthened with UHPFRC layers and steel bars are presented in Figure 12.

The experimental results of Figure 12 indicate that there is a positive agreement between the experimental results of the two identical specimens for all the examined cases. The values for the maximum load and the stiffness, which was calculated from the linear part of the load-deflection curve, together with the average results are presented in Table 4.

From the results of Figures 12 and Table 4, it is clear that the addition of UHPFRC layers at the tensile side of the RC beams resulted in a large increase of the stiffness of the RC beams, while the load carrying capacity was also increased. The addition of steel bars to the UHPFRC layer, resulted in a significant increase of the load carrying capacity. Thus, comparing the average curves, the load carrying capacity of the strengthened beams with UHPFRC layers and steel bars was increased by 90% compared to the load carrying capacity of the control beams.

The crack pattern and the failure mode of the existing RC beams and the strengthened beams, at the failure load (80% of the maximum load) are presented in Figures 13a-13d. The failure mode of beams P1 and P2 was identical. The failure mode of beam P1 is presented in Figure 13a. As shown in this figure, a crack in the middle of the span length was crucial for the failure of the beam. The first flexural cracks were visible when the load was equal to 24 kN, and the

crucial crack for the failure of the beam appeared when the load was equal to 31 kN in the middle of the span length. After this point, a localization of the damage could be distinguished while more flexural cracks propagated along the whole length of the beam. As shown in the same figure, a failure at the compressive side of the beam occurred during the testing. This failure started once the beam had reached its maximum load carrying capacity, and it was at the descending branch of the load-deflection curve. This resulted in the damage of the beam on both the compressive and the tensile sides at the end of the test. Identical was the failure mode of beam P2. The first minor cracks were visible for a value of load equal to 20 kN, while the crucial cracks start appearing at 25 kN. After this point, the damage localised, while more flexural cracks propagated progressively along the whole the length of the beam. Both the compressive and the tensile sides of the beam were damaged at the end of the test.

Identical was also the failure mode of beams U1 and U2. The first crack during the testing of beam U1 (Figure 13b), which was also crucial for the failure of the beam, was visible for a value of load equal to 32 kN on the UHPFRC layer and progressively propagated along the RC beam. During the testing, more flexural cracks propagated along the whole length of the beam. For a value of load equal to 48 kN and before the beam reached its maximum load capacity, a local de-bonding began at the interface. This local de-bonding can be attributed to the poor bonding at the interface between the UHPFRC layer and the existing beam at this area. From the examination of the specimen at the end of the test it was noticed that the roughness depth at this area was lower. As the beam reached its maximum load carrying capacity and was at the descending branch of the load-deflection curve, a failure at the compressive side of the beam commenced, which had as a result the damage of the compressive side at the end of the test. The failure mode of beam U2, is presented in Figure 13c. As can be seen in this figure, the bonding at the interface for beam U2 was effective. The first crack during the testing, start appearing for a value of load equal to 28 kN on the UHPFRC layer and progressively

propagated on the RC beam. During the testing and for the higher values of a load, more flexural cracks appeared on the strengthened beam. At the descending branch of the load-deflection curve, a failure at the compressive side commenced.

The failure mode of beams UB1 and UB2 was identical but different compared to beams P1,P2,U1 and U2. In Figure 13d the failure mode of beam UB1 is presented. Crucial for the failure of the beam was the failure at the compressive side of the beam. Accordingly, once the maximum load carrying capacity of the beam at the compressive side was reached, the damage at this side commenced and the beam could not carry any more load. The steel bars, on the other hand, improved the load carrying capacity of the strengthened beam significantly. The first cracks during the testing start appearing when the value of the load was equal to 57.5 kN on the RC beam, and once the beam had reached its maximum load carrying capacity, a single crack progressively propagated along the UHPFRC layer. This crack resulted in the failure of the layer at a later stage. The bonding at the interface was strong, and there was not any debonding even at the failure of the beam. The failure mode of beam UB2 was identical to beam UB. Therefore, the failure at the compressive side of the beam was crucial for the failure of the strengthened beam. The first cracks during the testing could be distinguished for a value of load was equal to 65 kN; after this point, more cracks propagated along the whole length of the beam. At the point at which the beam had reached its maximum load carrying capacity, the crack in the middle of the span length spread along the UHPFRC layer. Therefore, it led to the progressive failure of the layer.

During the testing of the strengthened beams, measurements were taken for the slip at the interface in different positions (Figures 10a and 10b). Due to the local de-bonding at the interface of beam U1, the measurements of slips were affected. Therefore, these measurement were ignored. The results for the load versus the slip for beam U2 are presented in Figure 14.

The slip close to the supports was equal to zero. Hence, slips were recorded at the positions of the LVDTs 2, 3, 4, 7 and 8 (see Figures 10a and 10b), areas where the interface stresses were significantly higher. Low readings, were recorded at the position of LVDT 5.

The results for the load versus the slips for the beams UB1 and UB2 are presented in Figures 15a-15b.

From the measurements of slip for beam UB1, it was noticed that the slip close to the supports was almost zero, and small values were recorded at the positions of the LVDTs 5 and 7. By contrast, values between 0.13 mm and 0.15 mm were recorded at the positions of LVDTs 3 and 4, which are located close to the two loading points. Finally, a high value of the slip was recorded at the position of LVDT 8, located in the area between the two loading points, and a value of the slip equal to 0.32 mm was also recorded at the position of LVDT 2. The measurements of beam UB2 indicated that the slip in the area close to the supports was equal to zero, and that the higher values were obtained in the area close to the two loading points (positions of LVDTs 3 and 4). The maximum value of slip was recorded at the position of LVDT 8 in between the two loading points. The difference in values of slip is attributed to the variation of the shear strength which is considerably affected by the normal to the interface stress. In case of high normal to the interface stress, such as the areas near the support, the shear strength is higher than the shear stress and therefore interface slip is prevented. Also, the difference in the values of slip can be attributed to the different level of preparation of the interface. Despite the fact that in the present study the sand patch method was used to quantify the concrete surface texture, it is possible that there were local imperfections and variations of the level of roughening along the interface.

In existing codes [29, 30], limit state values for the design of composite structures, are proposed. According to the Greek Code of Interventions [29], a maximum slip value of 0.2 mm is proposed for the immediate occupancy performance level, while values of 0.8 mm and 1.5

mm are proposed for the life safety performance level and the collapse prevention performance level, respectively. According to the fib Bulletin 43 [30] on the other hand, a maximum interface slip of 0.2 mm is suggested for the serviceability limit state and 2.0 mm for the ultimate limit state. The measurements of slip at the interface of the present study indicate an effective bonding between the UHPFRC layer and the existing RC beam. Hence, in all the examined cases and for both the examined techniques (with and without steel bars), the recorded values in different positions were lower than 0.35 mm which according to the Greek Code of Interventions [29], corresponds to the life safety performance level. Since, the values of slippage are highly affected by the shear stress, the bond at the interface and the crack development, it is assumed that the recorded values of slip would not be much dissimilar for member for higher dimensions.

The effective bonding between the UHPFRC layer and the existing RC beams is also evident comparing the recorded values of slip at the interface, with the reported values in the literature for concrete to concrete interfaces. Tsioulou et al. [20], recorded values of slip equal to 1.1 mm for concrete to concrete interfaces for strengthening of full scale RC beams with RC layers at tensile side and along the whole length of the beam. This value corresponds to the collapse prevention performance level and it is significantly higher compared to the recorded values of the present study. It is worth mentioning that the loading conditions, the loading rate and the dimensions of the specimens of this study were identical with the present study. Therefore, the results are comparable.

2.6 Evaluation of the interface characteristics

In Figure 16, the results for the shear stress versus the interface slip together with the average curve are presented. In this figure only the results of the successful tests are presented. Some of the examined specimens failed in an undesired way (for example due to significant flexural

stress) and these results were eliminated from the graphs. However, several examined specimens were successfully tested with high shear stresses acting at the interface and without any significant flexural stresses which was evidenced by the load slip results and by the failure mode. In Figure 17a the failure mode of a successful test with high shear stresses is presented, while in Figure 17b is presented an example of the failure mode of an successful test. The experimental setup of the present investigation has been used by Vitzilaiou [32] for the investigation of conventional concrete to concrete interfaces. Finally, it worth mentioning that as the number of the tests is quite low, they can be used to give an indication of the interface conditions. Further extensive experimental study is required in order to evaluate the interface characteristics.

According to Eurocode 2 [21], shear strength of an ordinary concrete can be calculated using Equation 1.

$$\tau_{ud} = c \cdot f_{ctd} + \mu \cdot \sigma_N \leq 0.5 \cdot v \cdot f_{cd} \quad (1)$$

Where: τ_{ud} is the shear strength at the interface; c is the adhesion factor; μ is the coefficient of friction; σ_N is the external normal to the interface stress; v is equal to $0.6 \cdot (1 - f_{ck}/250)$; f_{ck} is the characteristic compressive strength of the concrete; f_{ctd} is the design tensile strength of concrete with the lower strength (between the old and the new concrete) and is given by its concrete tensile strength; $\gamma_c = 1.5$ for concrete and f_{cd} is the concrete compressive strength and is given by f_{ck}/γ_c .

Coefficients of friction and cohesion were calculated using Equation 1. Cohesion ($c \cdot f_{ctd}$) was considered as the shear stress at the interface for slip value equal to 0.01 mm following the available code provisions (GRECO [29] , CEB Fib Model Code [31]). Coefficients of friction were then calculated using equation 1 and by substituting cohesion and maximum shear strength values obtained from the push-off tests while σ_N is the value of the externally applied

normal to the interface stress which in the current study was equal to 1 MPa. The same value of stress has also been adopted by Vitzilaiou [32], for the investigation of the characteristics of RC interfaces through push off tests, leading to comparable results.

The interface characteristics for all the examined specimens calculated using the procedure aforementioned are presented in Table 5. Based on these results a value of 1 was calculated for the coefficient of friction and a value of 1.8 MPa for the cohesion. In Eurocode 2 [21], and for normal concrete, there are suggested values for both the coefficients of friction and coefficient of adhesion. More specifically, for a rough interface, a value of 0.45 is proposed for the coefficient of adhesion and a value of 0.7 is proposed for the coefficient of friction. It can be noticed that the obtained values of the present research were found to be higher compared to the proposed values in Eurocode 2 [21] for concrete to concrete interfaces. This is in agreement with the measurements of the slip at the interface of the strengthened beams, in which case, better connection between UHPFRC and concrete was identified compared to concrete to concrete interfaces.

Based on the results of the present investigation and for the numerical modeling of the examined technique, a value of 1 will be used for the coefficient of friction and a value of 1.8 MPa for the cohesion.

3. The numerical modelling of Ultra High Performance Fiber Reinforced Concrete (UHPFRC)

3.1 The modelling of the materials

In the experimental investigation, the existing RC beams were strengthened with a layer depth of 50 mm, while the diameter of the steel bars was 10 mm, while a fiber content of 3% was used for the preparation of the UHPFRC. Based on Paschalis and Lampropoulos [14] the optimum fiber content of UHPFRC, in terms of workability and mechanical performance, was

achieved for a fiber content in the range of 3-4%. Preliminary studies have been conducted using UHPFRC layers with fiber contents 3% and 4% and it was found that the results are not significantly affected by the fiber content. Therefore, in the present study are examined the most significant parameters which were found to be the thickness and the steel ratio.

The selection of the appropriate dimensions of the layer can be related with parameters such as the geometry of the existing members, the decision to increase or not the stiffness of the existing members and the type and the dimensions of the fibers. Based on the target behavior of the strengthening technique, it is of high importance that the optimum decision for the selection of the appropriate layer depth and the amount of reinforcement is taken. In the present section, different alternatives for the selection of the appropriate layer depth and the amount of reinforcement of the layer are investigated numerically. The finite element model used in the present investigation, has been validated according to the experimental results of the full-scale beam testing.

For the finite element analysis, ATENA software was used. Concrete was simulated with an eight node element, with nonlinear behavior and softening branches under both tension and compression, using SBETA constitutive model [33] and the properties of concrete of a previous section were adopted for the numerical modeling of concrete. The ascending compressive branch is based on the formula recommended by CEB-FIP model code 90 [34] while its softening law is linearly descending from the peak stress until a limit compressive strain, which was defined by the plastic displacement and the band size, using fictitious compression plane model. The constitutive model in tension and compression adopted in ATENA software is presented in Figure 18. For the numerical modelling of UHPFRC the material properties of the previous section were adopted. Therefore, a compressive strength of 136.5 MPa and Young's modulus equal to 51 GPa were used for the modelling in compression using the SBETA constitutive model. In tension, the response of UHPFRC was considered linear up to stress

level equal to 5 MPa, and it was modelled with an elastic behavior up to initiation of the microcracking, followed by a second part into the phase of strain hardening with microcracking. After the formation of the macrocrack at the ultimate resistance, there is the strain softening phase which was modelled with a bi-linear model. The stress-strain and stress-crack opening behaviour of UHPFRC in tension have been investigated in depth by Paschalis and Lampropoulos [3]. Based on this study, and for a fiber content 3%, the most appropriate model to simulate the stress-crack opening behaviour was the one using a bi-linear function.

The tensile function adopted in the Atena is presented in Figure 19. Finally, for the modelling of UHPFRC, the shrinkage of the material was considered using a negative volumetric strain value to the UHPFRC elements. More specifically, based on the measurement of shrinkage of a previous study [16] an ultimate value of shrinkage equal to 565 microstrain for a fiber content of 3%, was applied to the elements of the UHPFRC layers. The steel bars, were simulated using linear elements with bilinear behavior and the yield stress of the steel bars was 500 MPa, while the cover of the steel bars was 25 mm. The interface between the initial beam and the UHPFRC layer was modelled using two dimensional contact elements with a coefficient of friction equal to 1 and cohesion equal to 1.8 MPa. These values were obtained from the push off tests of the previous section.

The mesh size was approximately two times the maximum aggregate size and was selected based on the proposed optimum mesh sizes [35]. However, when the Atena software [33] is used the results are not significant influenced by the FE mesh size.

3.2 Validation of the numerical model

In Figure 20, a comparison between the numerical and the experimental results for the different strengthening configurations is presented.

The results of Figure 20 indicate a positive agreement between the numerical and the experimental results. Hence, similar elastic and post elastic behavior can be distinguished in all the examined cases and similar values for the maximum load. However, it can be noticed that the post peak branch of strengthened beam with layers and steel bars drops more suddenly compared to the numerical results. This can be attributed to sudden failure of the compressive side of the beams of the experimental investigation once the maximum compressive strength of the compressive side was reached. In Table 6, the numerical and the experimental results for the maximum load are presented.

The results of Table 6 indicate positive agreement between the experimental and the numerical results. The crack pattern and the strain distribution at the maximum load is presented in Figures 21a-21c.

The results of Figures 21a and 21b indicate high values of strain and localization of the damage at the tensile side of the beams and in the middle of the span length. On the contrary, from Figure 21c it is clear the steel bars in the layer had as result a different response of the strengthened beam and the layer was in tension along the whole length, which indicates the effectiveness of steel bars to increase the resistance to the imposed loads. Also, high values of strain can be distinguished at the compressive side. This is in agreement with the failure mode of the strengthened beams of the experimental investigation.

3.3 Strengthening with different layer depths and different amounts of reinforcement of the layer

Crucial parameters which affect the performance of the examined technique are the depth of the layer and the amount of the reinforcement of the layer. In the present investigation, three different layer depths were examined, namely 30 mm, 50 mm and 70 mm, while the layers were reinforced with steel bars with diameters of 10 mm and 16 mm. The grade of the steel

bars in all the examined cases was the same with the experimental investigation, namely B 500 C. All the numerical results for the different diameters and the different depths are presented in the same graph in Figure 22 and the results of for the yield and the maximum load are presented in Table 7. The increment of the yield and maximum load for the different layer depths and the different diameter of steel bars are presented in Figure 23.

From the numerical results of the present investigation it is clear that the amount of the reinforcement of the layer is a very important parameter affecting the performance of the strengthened beams. Also, in terms of the maximum resistance to the imposed loads, it seems that the amount of reinforcement of the layer is a more important parameter than the depth of the layer. Therefore, it can be noticed that the performance of the strengthened RC beam with a 30 mm layer and steel bars with a diameter of 16 mm was better compared to the performance achieved for strengthening with UHPFRC layers with depths 50 mm and 70 mm and steel bars with a diameter of 10 mm. As expected, the optimum performance was achieved for the 70 mm layer depth and steel bars with a diameter of 16 mm, in which case the maximum load was found to be equal to 156.7 kN. However, it should be noted that before the decision for the selection of the appropriate layer depth, parameters such as the geometry of the existing member, the minimum required cover of the reinforcement and the type and the dimension of the fibers, should be taken into consideration.

4. Conclusions

In the present study an extensive experimental and numerical investigation on the performance of UHPFRC for the strengthening of RC beams was conducted. UHPFRC was applied for the strengthening of full scale RC beams using different configurations. During the testing, measurements for the slip at the interface between UHPFRC and concrete were recorded. An additional investigation was conducted on the study of interface between UHPFRC and

concrete through push-off tests. Finally, certain significant parameters, such as the effect of the layer depth and the amount of the reinforcement of the layer were investigated numerically.

Based on the experimental results of the present study the following conclusions can be drawn:

- The addition of UHPFRC layers at the tensile side of the RC beams resulted in a large increase in the stiffness of the RC beams and the formation of the cracks was delayed while the load carrying capacity was also slightly increased.
- The addition of steel bars to the UHPFRC layer had as a result a big increase in the load carrying capacity of the strengthened beams. Therefore, the average maximum load of the strengthened beams with UHPFRC layers and steel bars was increased by 87%, with the addition of steel bars to the layer. Consequently, this technique can be applied in cases that the target behavior of the strengthening technique is the high resistance to the imposed loads.
- The bonding between UHPFRC and concrete was effective and small values of slip at the interface were recorded. Also, comparing the recorded values of slip with reported values in the literature for concrete to concrete interfaces, it was noticed that the values of slip for UHPFRC to concrete interfaces were significant lower. This indicates a more effective bonding between UHPFRC and concrete compared to concrete to concrete interfaces. However, further investigation on the interface characteristics between UHPFRC and RC is considered necessary.
- The amount of reinforcement of the layer is an important parameter affecting the performance of the strengthened elements significantly. Hence, high load carrying capacity can be achieved with higher amount of reinforcement of the layer and even with lower layer depths.

Acknowledgements

The authors would like to express their gratitude to David Pope for his assistance during the testing, and they would like to acknowledge Sika Limited and Hanson Heidelberg Cement Group for providing raw materials.

References

- [1] Kang S.T., Lee Y., aPark Y.D., Kim J.K., Tensile fracture properties of an Ultra High Performance Fiber Reinforced Concrete (UHPFRC) with steel fibers, *Composite Structures*, 92 (1): (2010), 61-71.
- [2] Yoo Y., Shin H.O., Yang J.M., Yoon Y.S., Material and bond properties of Ultra High Performance Fiber Reinforced Concrete with micro steel fibers, *Composites Part B: Engineering*, 58: (2013), 122-133.
- [3] Paschalis S., Lampropoulos A., (2017), Fiber content and curing time effect on the tensile characteristics of Ultra High Performance Fiber Reinforced Concrete (UHPFRC), *The Fib Structural Concrete Journal*, 18 (4), pp. 577-588, ISSN: 1751-7648
- [4] Neocleous K., Tlemat H., Pilakoutas K., Design issues for concrete reinforced with steel fibres including fibres recovered from used tires, *Journal of Materials in Civil Engineering ASCE*, 18 (5): (2006), 677 – 685.
- [5] Nicolaidis D., Kanellopoulos A., Petrou M., Savva P., Mina A., Development of a new Ultra High Performance Fibre Reinforced Cementitious Composite (UHPFRCC) for impact and blast protection of structures, *Construction and Building Materials*, 95: (2015), 667-674.
- [6] Ferrara L, Ozyurt N, di Prisco M., High mechanical performance of fibre reinforced cementitious composites: the role of "casting-flow induced" fibre orientation, *Materials and Structures*, 44 (1): (2011), 109-128.

- [7] Paschalis S., Lampropoulos A., Ultra High Performance Fiber Reinforced Concrete Under Cyclic Loading, *ACI Materials Journal*, 113 (4): (2016), 419-427.
- [8] Karihaloo B.L., Benson S.D.P., Alaei, F.J., CARDIFRC UK patent GB2391010 (2005).
- [9] Wille K. and Naaman A.E., Fracture energy of UHP-FRC under direct tensile loading, *Proceedings of Fracture Mechanics of Concrete and Concrete Structures-Recent Advances in Fracture Mechanics of Concrete-7*, Seoul, South Korea, 23-28 May 2010.
- [10] Tsioulou O., Lampropoulos A., Paschalis S., Combined Non-Destructive Testing (NDT) method for the evaluation of the mechanical characteristics of Ultra High Performance Fibre Reinforced Concrete (UHPFRC), *Construction and Building Materials*, 131: (2017), 66-77
- [11] Habel K., Viviani M., Denarie E., Bruhwiler E., Development of the mechanical properties of an Ultra-High Performance Fiber Reinforced Concrete (UHPFRC), *Cement and Concrete Research*, 36 (7): (2006), 1362-1370.
- [12] Benson S.D.P, Karihaloo B.L., CARDIFRC-Development and mechanical properties. Part III: Uniaxial tensile response and other mechanical properties, *Magazine of Concrete Research*, 57 (8): (2005), 433-443.
- [13] Paschalis S., Lampropoulos A., Size effect on the flexural Performance of UHPFRC, *Proceedings of THE 7th HPRCC Conference*, Stuttgart, Germany, 1-3 June 2015.
- [14] Paschalis S., Lampropoulos A., (2016), "Mechanical performance and cost correlation of Ultra High Performance Fiber Reinforced Concrete (UHPFRC)", *19th Congress of IABSE Stockholm 2016*, 21-23 September 2016
- [15] Habel K., Denarie E., Bruhwiler E., Structural response of elements combining Ultra-High-Performance Fiber Reinforced Concretes and Reinforced Concrete (2006). *Journal of Structural Engineering*, 132 (11): (2006), 1793-1800

- [16] Lampropoulos A., Paschalis S., Tsioulou O., Dritsos S., Strengthening of reinforced concrete beams using ultra high performance fibers reinforced concrete (UHPFRC), *Engineering Structures*, 106: (2015), 370-384.
- [17] Bruhwiler E., Denarie E., Rehabilitation of concrete structures using Ultra-High Performance Fibre Reinforced Concrete, *The Second International Symposium on Ultra High Performance*, Kassel, Germany, 5-7 March
- [18] Safdar M., Takashi Matsumoto T., Kakuma K, Flexural behavior of reinforced concrete beams repaired with Ultra High Performance Fiber Reinforced Concrete (UHPFRC), *Composite Structures*, 157: (2016), 448-460.
- [19] Talayeh Noshiravani and Eugen Bruhwiler, Experimental Investigation on Reinforced Ultra- High Performance Fiber-Reinforced Concrete Composite Beams Subjected to Combined Bending and Shear, *ACI Structural Journal*, 110 (2):(2013), 251-262
- [20] Tsioulou, O., Lampropoulos, A., Dritsos, S., Experimental investigation of interface behavior of RC beams strengthened with concrete layers, *Construction and Building Materials*, 40: (2013), 50-59.
- [21] Eurocode 2, CEN En 1992-1-1, Eurocode 2: Design of concrete structures –Part 1-1: General rules and rules for buildings. Brussels: European Committee for Standardization; 2004
- [22] fib Bulletin No 55. Model Code 2010. Lausanne: International Federation for Structural Concrete (fib); 2010.
- [23] Technical Chamber of Greece, (2004). Strengthening of structures against seismic loading, Available at: <http://lee.civil.ntua.gr/pdf/dimosiefseis/vivlia/enisxisi.pdf>, [Accessed 12-8-2017].

- [24] Trucy I., Dobrusky S., Bonnet E., Ultra-high performance shotcrete: yes we can!, proceedings of UHPFRC 2017 Designing and Building with UHPFRC: New large-scale implementations, recent technical advances, experience and standards, 2017, pp 154 – 163,
- [25] Ductal, Innovation: Ductal Shotcrete the first sprayed UHPC Accessed on 25-6-2018 at <https://www.ductal.com/en/engineering/innovation-ductalr-shotcrete-first-sprayed-uhpc>
- [26] Skazlic M., Skazlic Z. ; and J. Majer J., Application of High Performance Fibre Reinforced Shotcrete for Tunnel Primary Support, 10th International Conference on Shotcrete for Underground Support, Whistler, 2006. p. 206-214.
- [27] BS EN 12390-3:2009, Testing hardened concrete-Part 3: Compressive strength of test specimens
- [28] BS 4449:2005. Steel for the reinforcement of concrete. Weldable reinforcing steel. Bar, Coil and Decoiled product. Specification, BSI.
- [29] Greek Retrofitting Code, (GRECO) Greek Organization for Seismic Planning and Protection, Athens, Greek Ministry for Environmental Planning and Public Works, 2013 (in Greek)
- [30] fib Bulletin No 43, Structural Connections for precast concrete buildings, Lausanne, International Federation for Structural Concrete, 2008
- [31] CEB-FIP Model Code 90, design code, fib Fédération internationale du béton, 1993
- [32] Vitzilaiou, E., Fundamental Mechanisms of Load Transfer in Reinforced Concrete Interfaces under Monotonic and Cyclic Loading (in Greek), PhD Thesis, National Technical University of Athens, Athens, Greece, 1986
- [33] Cervenka V., Jendele L., Cervenka J., ATENA Program Documentation: Part 1 Theory. Prague, Czech Republic; 2013

[34] Model Code 1990,CEB-FIP, London(UK), Thomas Telford; 1993

[35] Bazant Z.P., Oh B.H., Crack band theory for fracture of concrete. *Materials and Structures*, 16: (2013), 155–177.

Figure Captions

Figure 1 Geometry and reinforcement of the initial RC beams

Figure 2 Geometry and reinforcement of the strengthened beams with UHPFRC layers and UHPFRC layers and steel bars

Figure 3 Geometry and experimentl setup for the push off tests

Figure 4 Roughening of the surface with a pistol grip needle scaler

Figure 5 Preparation of the beams: a) beam ready for the casting of the layer b) reinforcement of the layer c) casting of the layers

Figure 6 Application of UHPFC layers in real practice

Figure 7 a) Dimensions of the dog-bone shaped specimens b) experimental setup for the tensile tests

Figure 8 Experimental results of the direct tensile tests of UHPFRC

Figure 9 Experimental setup for the four point loading tests

Figure 10 a) Positions of the LVDTs for the measurement of slips on side 1 b) positions of the LVDTs for the measurement of slips on side 2 c) LVDT used for the measurement of slip at the interface

Figure 11 Experimental setup for the push off tests

Figure 12 Load-deflection results for all the examined beams

Figure 13 Failure mode of: a) beam P1 b) beam U1 C) beam U2 c) beam UB1

Figure 14 Load versus slip in different positions of beam U2

Figure 15 a) Load versus slip in different positions of beam UB1 b) load versus slip in different positions of beam UB2

Figure 16 Shear stress versus interface slip from the push off tests

Figure 17 a) Failure mode of a successful push off test b) Example of the failure mode of an unsuccessful push off test

Figure 18 Constitutive model in tension and compression adopted in ATENA software

Figure 19 Tensile function adopted in ATENA software for the UHPFRC

Figure 20 Numerical versus experimental results for the initial beams, the beams strengthened with UHPFRC layers and the beams strengthened UHPFRC layers and steel bars

Figure 21 Crack Pattern at the maximum load for: a) the control beam b) the beam strengthened with UHPFRC layer c) the beam strengthened UHPFRC layers and steel bars

Figure 22 Load versus deflection results for different layer depths and different diameters of the steel bars

Figure 23 Increment of the yield and the maximum load for the different layer depths and the different diameters of the steel bars

Figure Captions

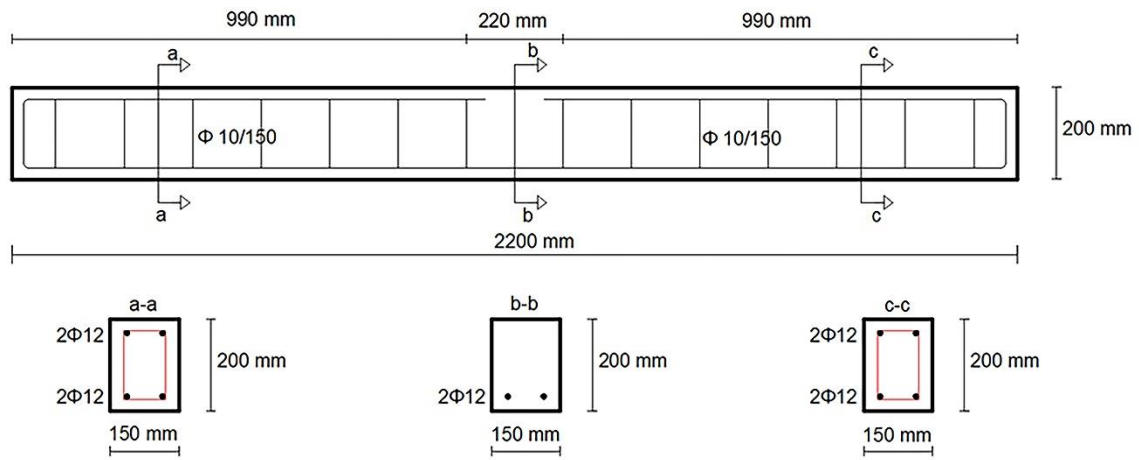


Figure 1 Geometry and reinforcement of the initial RC beams

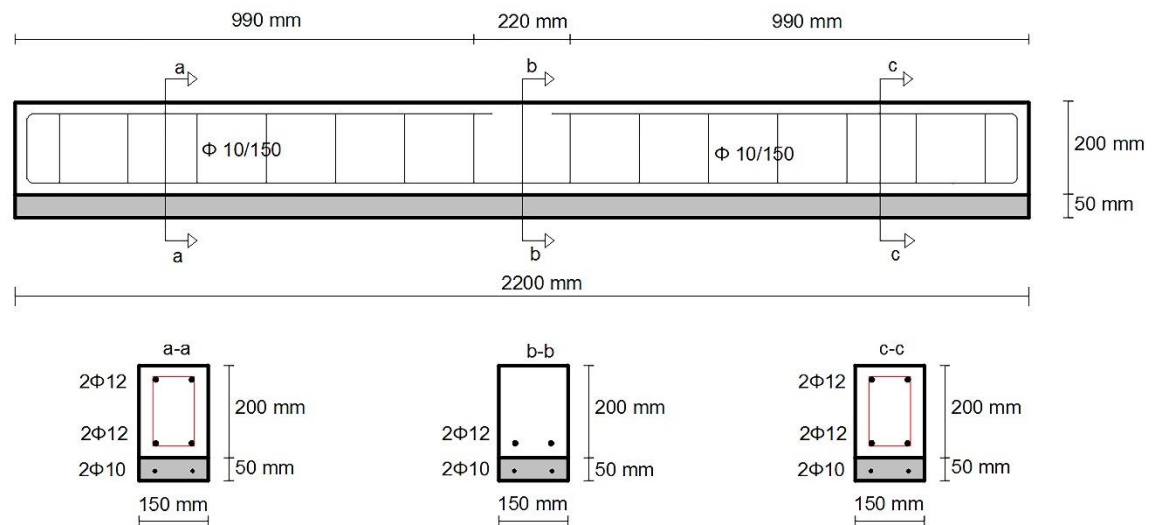


Figure 2 Geometry and reinforcement of the strengthened beams with UHPFRC layers and steel bars

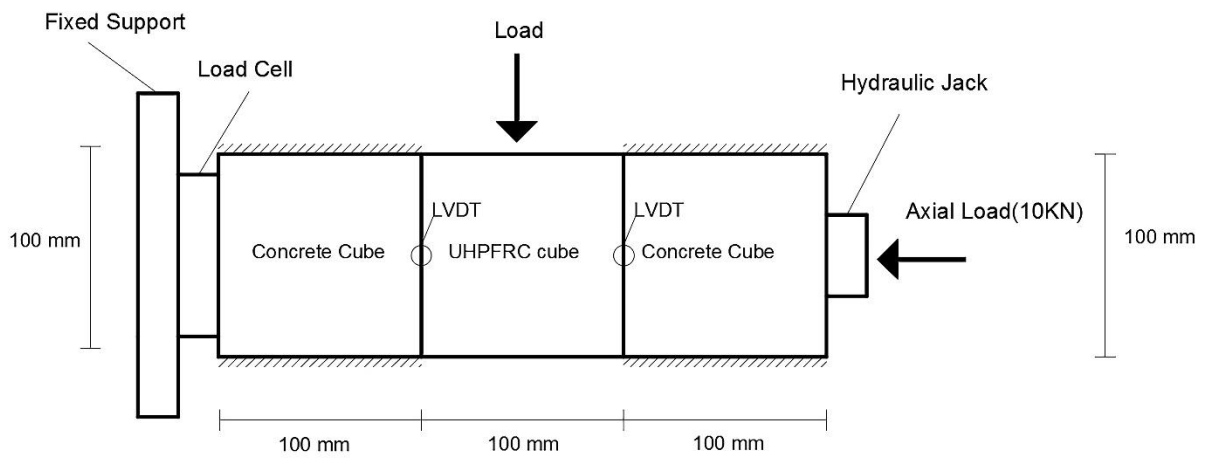


Figure 3 Geometry and experimentl setup for the push off tests



Figure 4 Roughening of the surface with a pistol grip needle scaler



a



b)



c)

Figure 5 Preparation of the beams: a) beam ready for the casting of the layer b) reinforcement of the layer c) casting of the layers

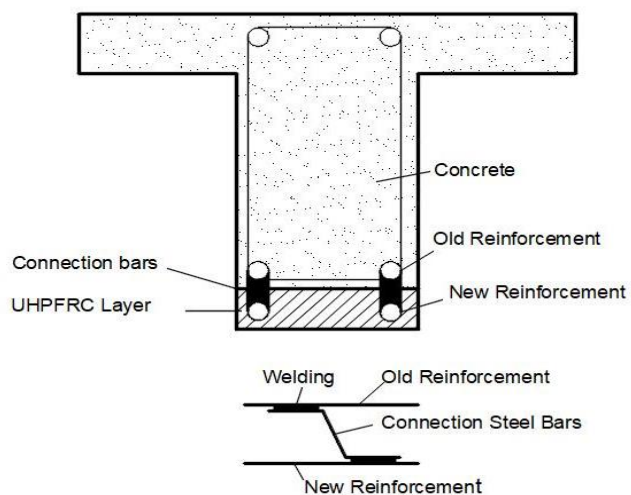
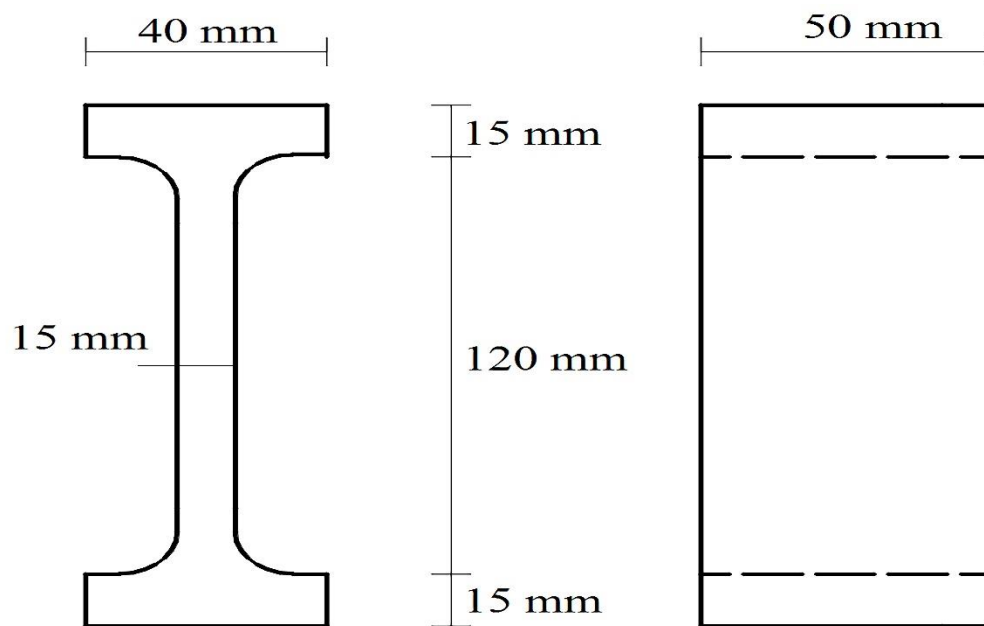


Figure 6 Application of UHPFRC layers in real practice



a



b

Figure 7 a) dimensions of the dog-bone shaped specimens b) experimental setup for the tensile tests

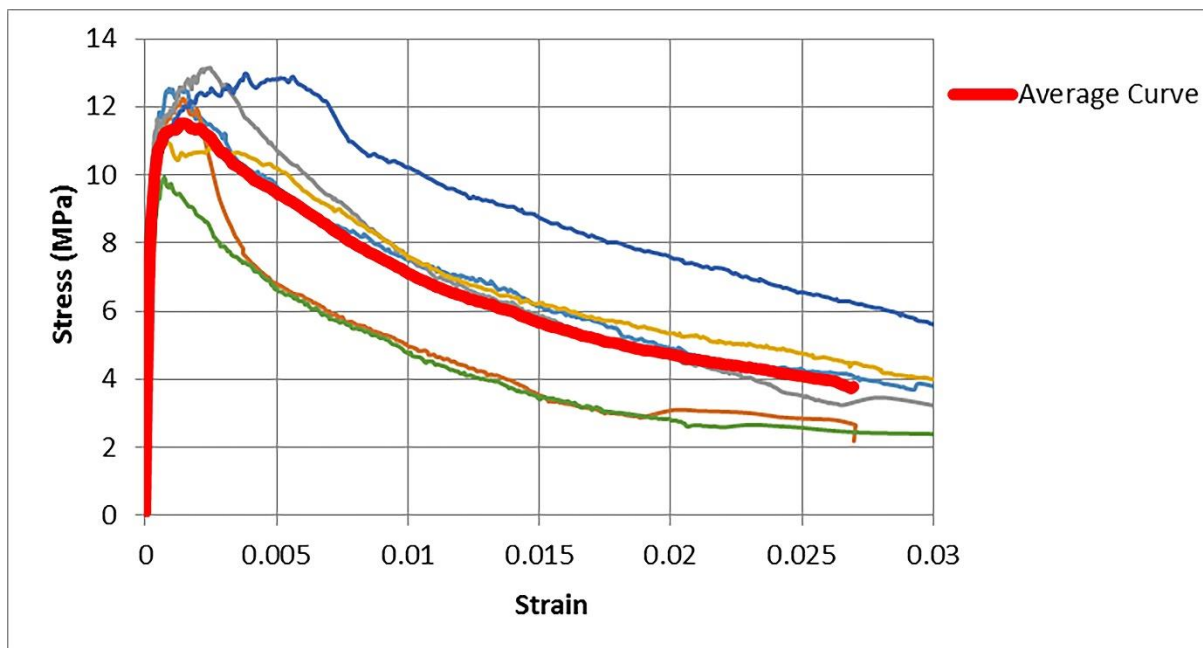
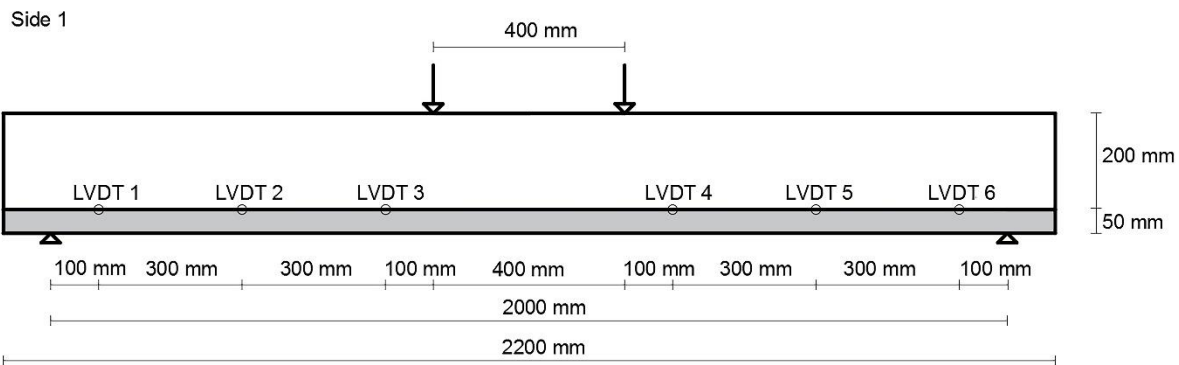


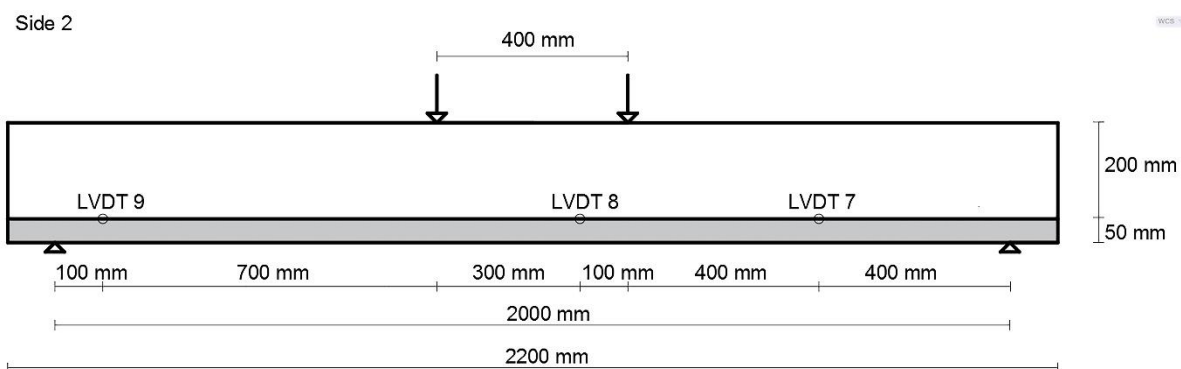
Figure 8 Experimental results of the direct tensile tests of UHPFRC



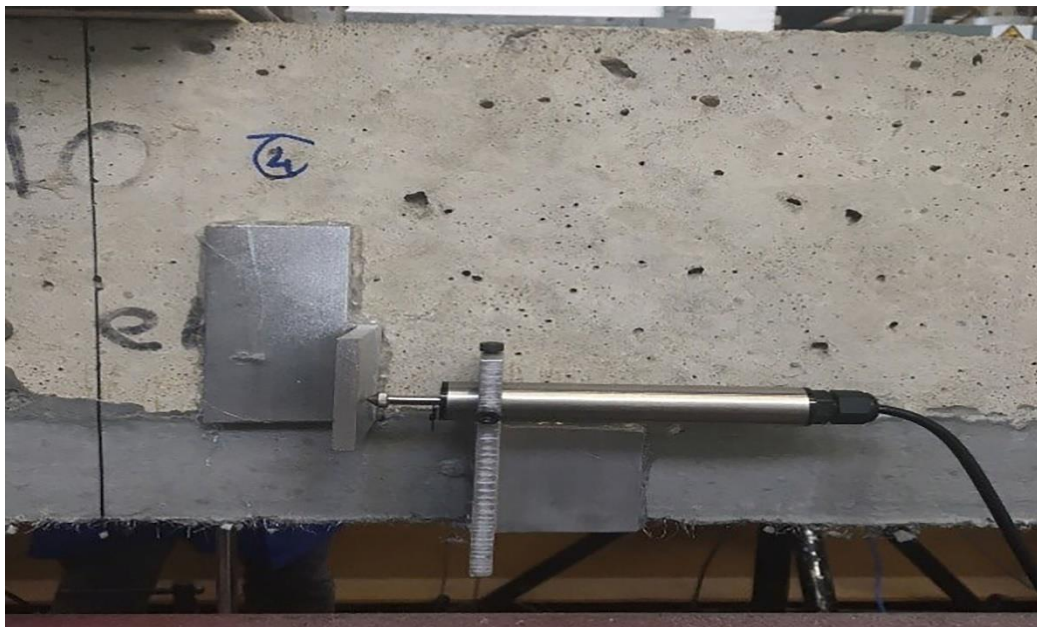
Figure 9 Experimental setup for the four point loading tests



a



B



C

Figure 10 a) Positions of the LVDTs for the measurement of slips on side 1 b) positions of the LVDTs for the measurement of slips on side 2 c) LVDT used for the measurement of slip at the interface

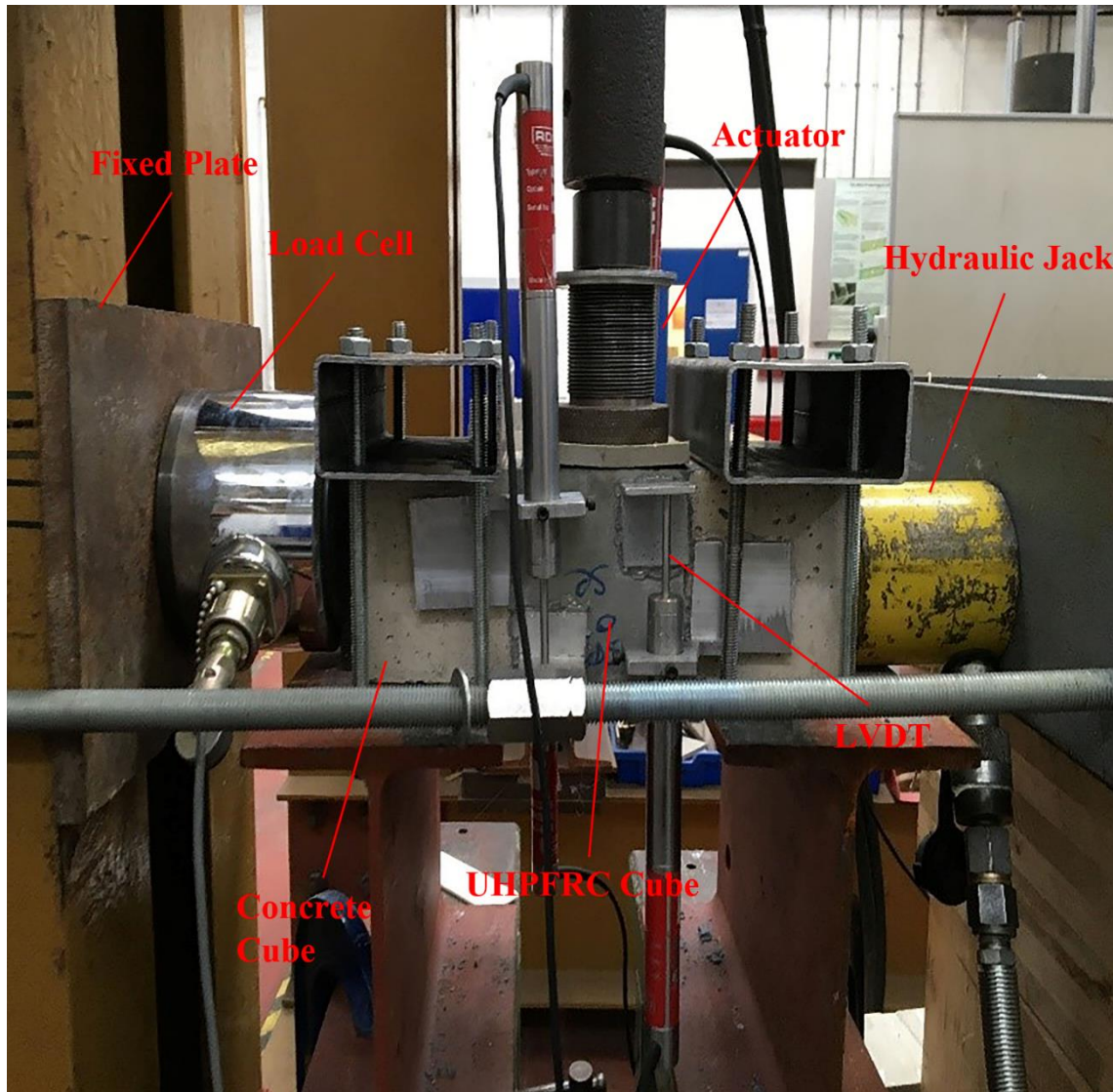


Figure 11 Experimental setup for the push off tests

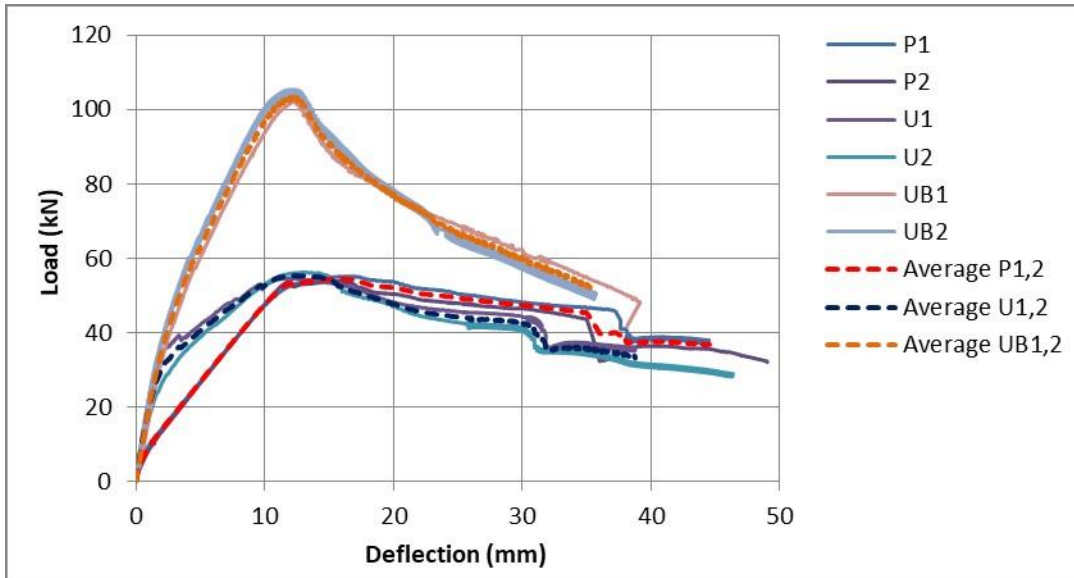
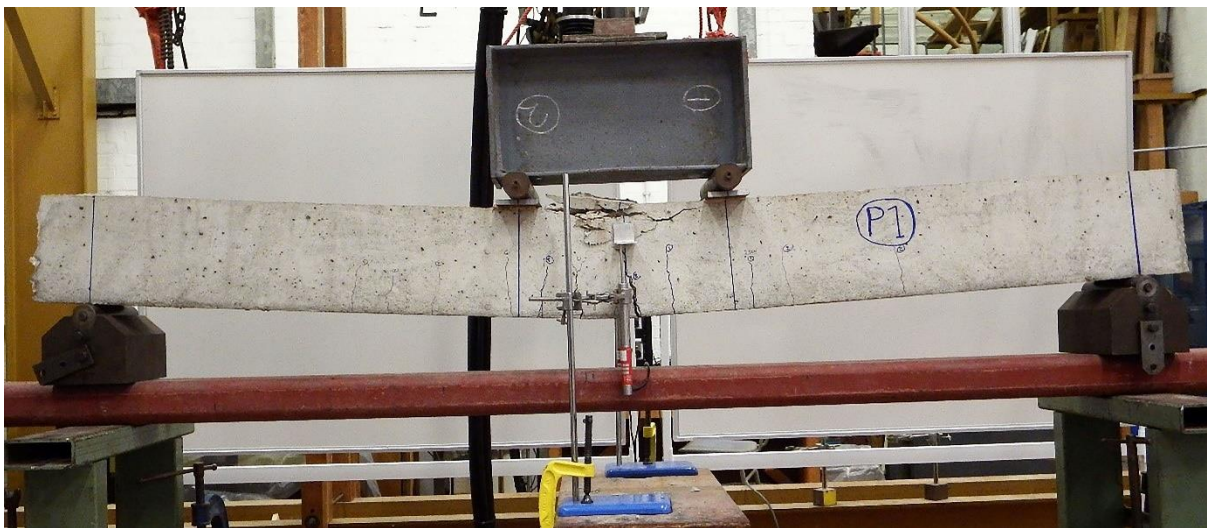


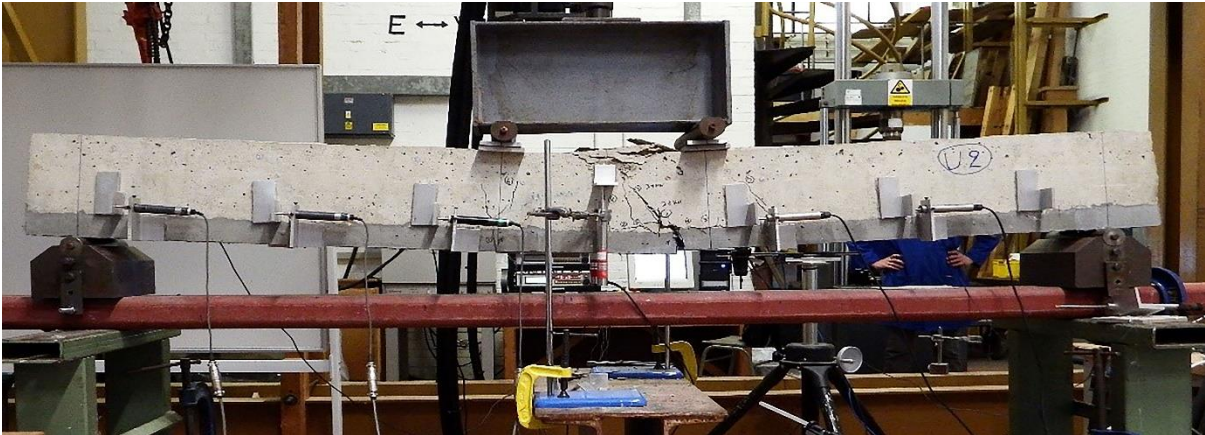
Figure 12 Load-deflection results for all the examined beams



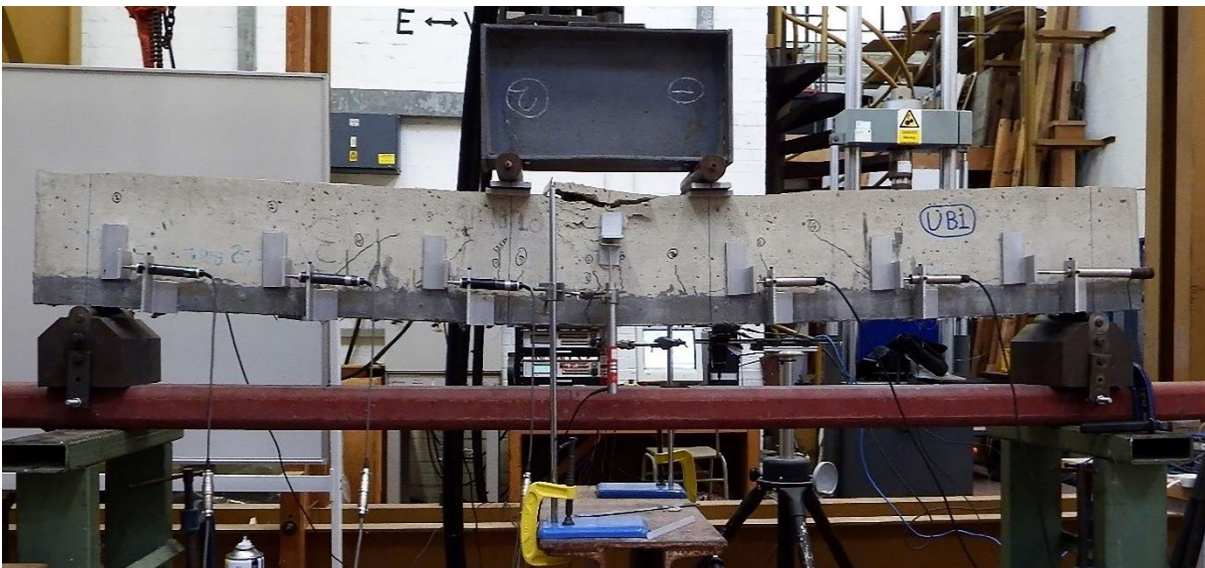
a



b



c



d

Figure 13 Failure mode of: a) beam P1 b) beam U1 C) beam U2 c) beam UB1

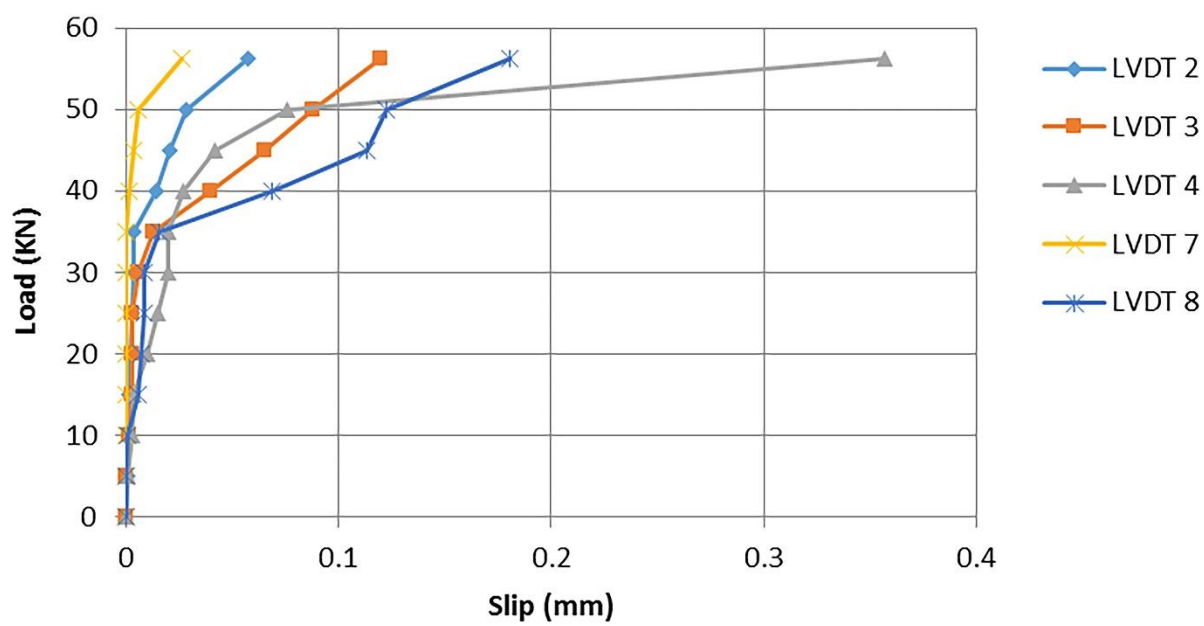
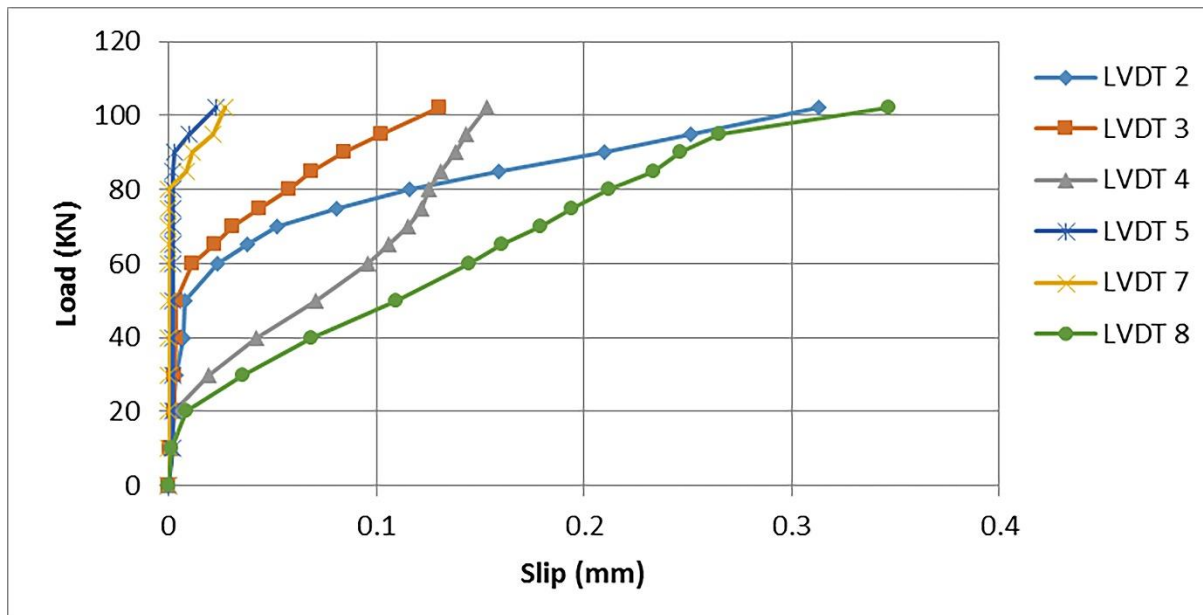
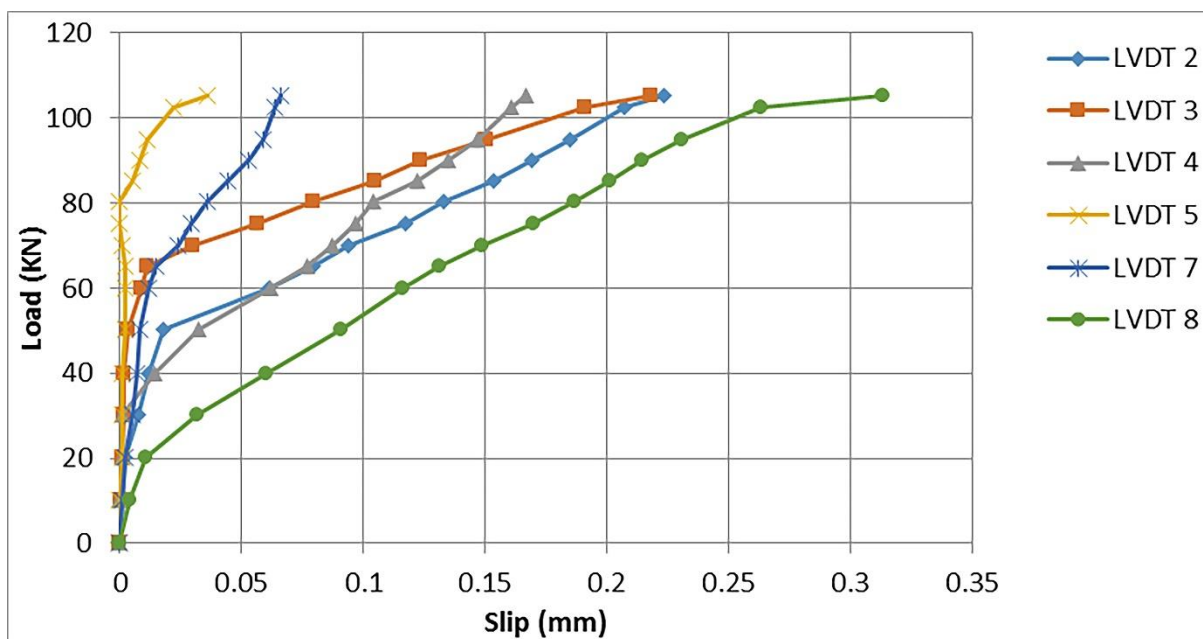


*Figure 14 Load versus slip in different positions for beam U2



a



b

Figure 15 a) Load versus slip in different positions for beam UB1 b) load versus slip in different positions for beam UB2

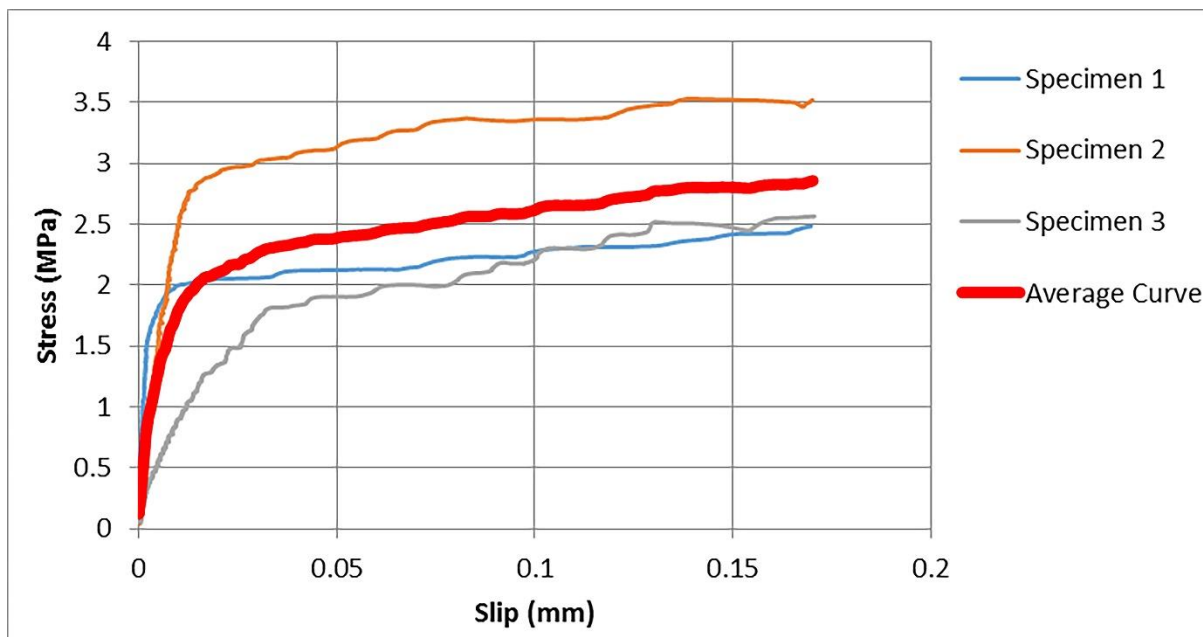
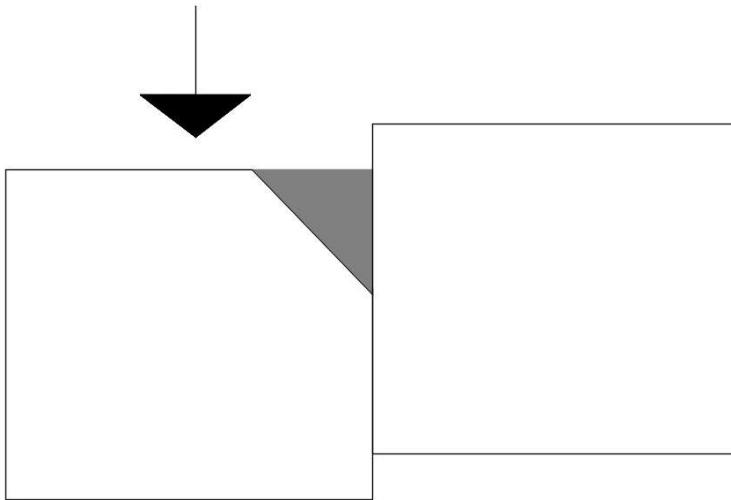


Figure 16 Shear stress versus interface slip from the push off tests



A



B

Figure 17 a) Failure mode of a successful test b) Example of the failure mode of an unsuccessful test

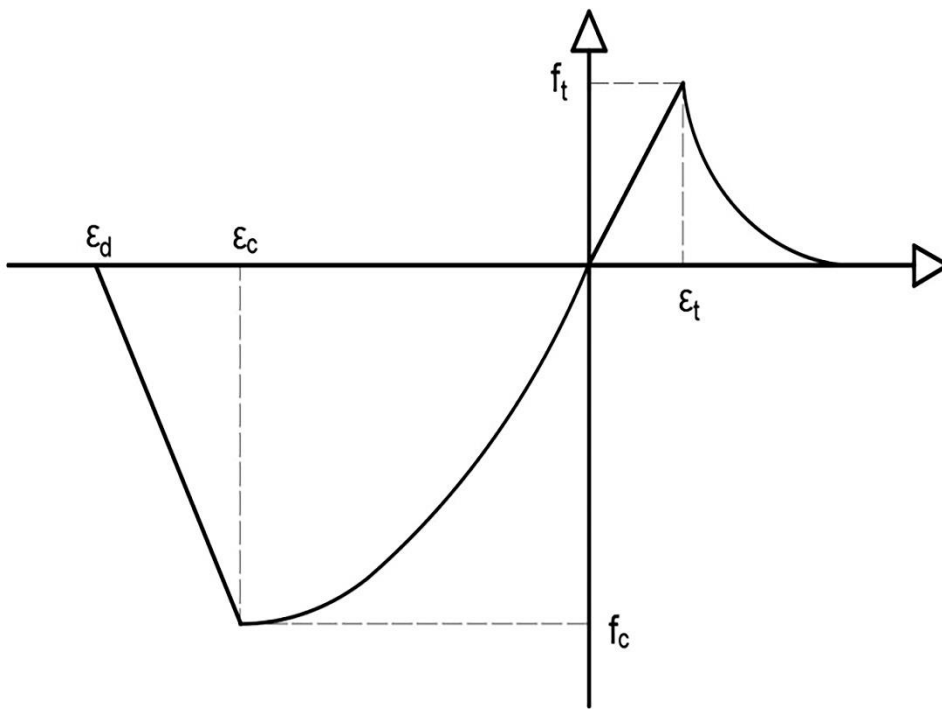


Figure 18 Constitutive model in tension and compression adopted in ATENA software

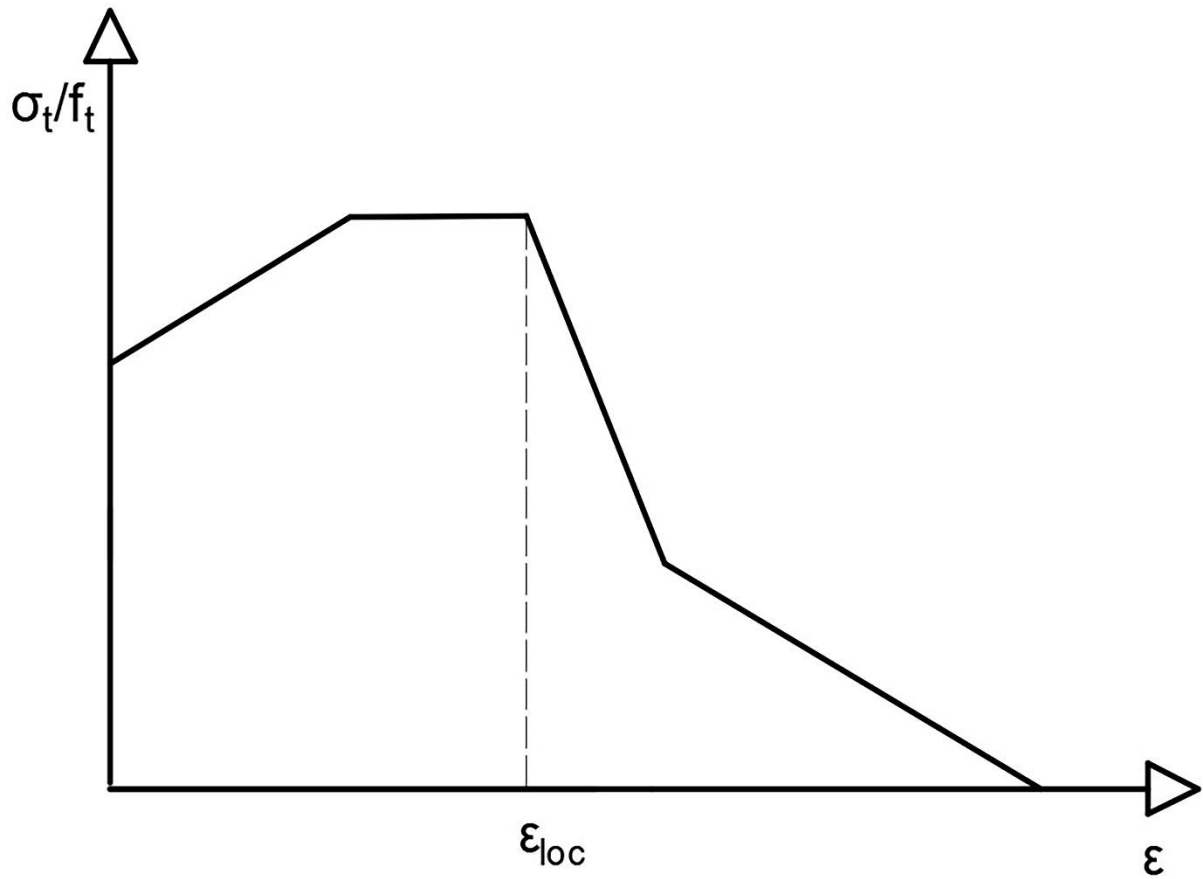


Figure 19 Tensile function adopted in ATENA software for the UHPFRC

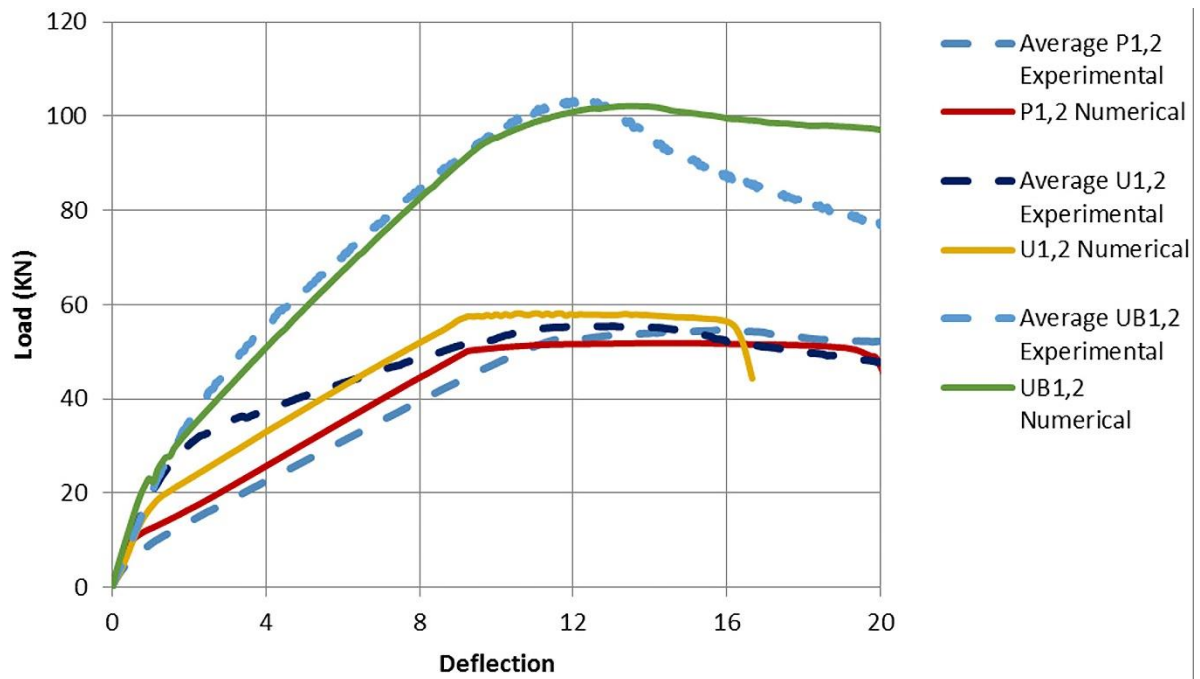
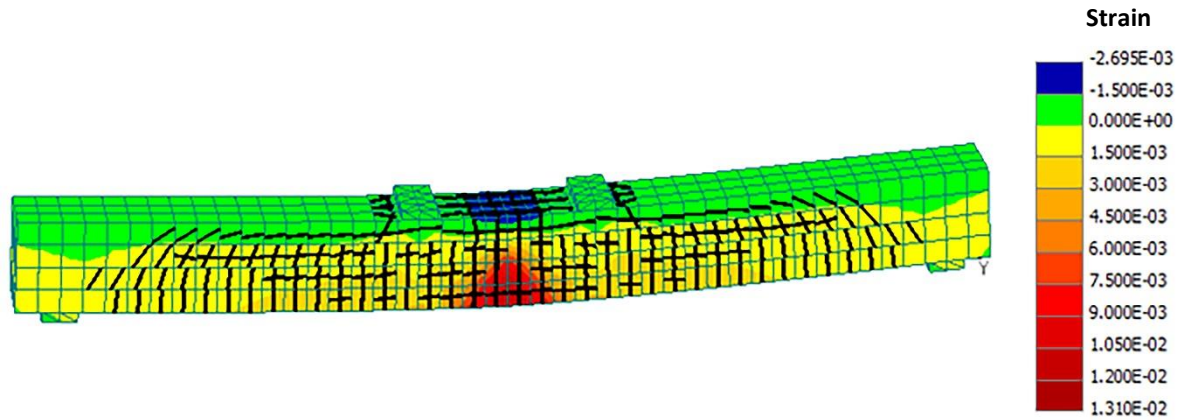
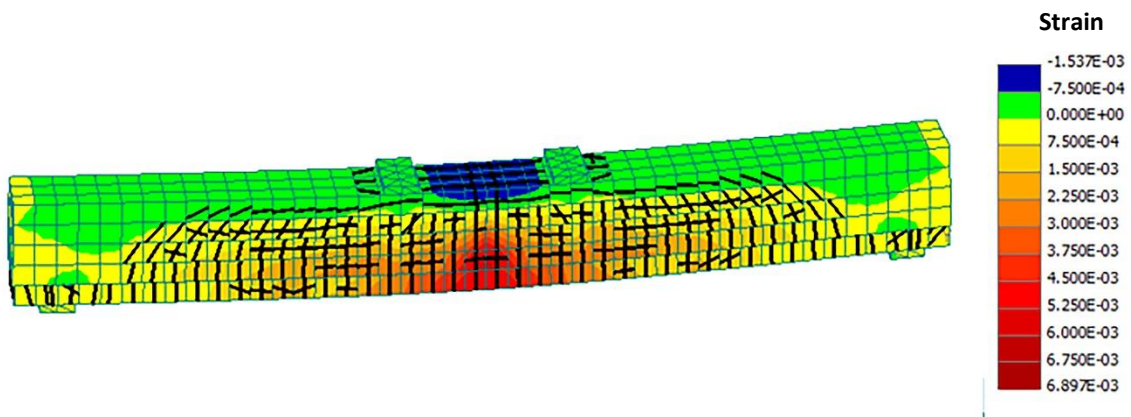


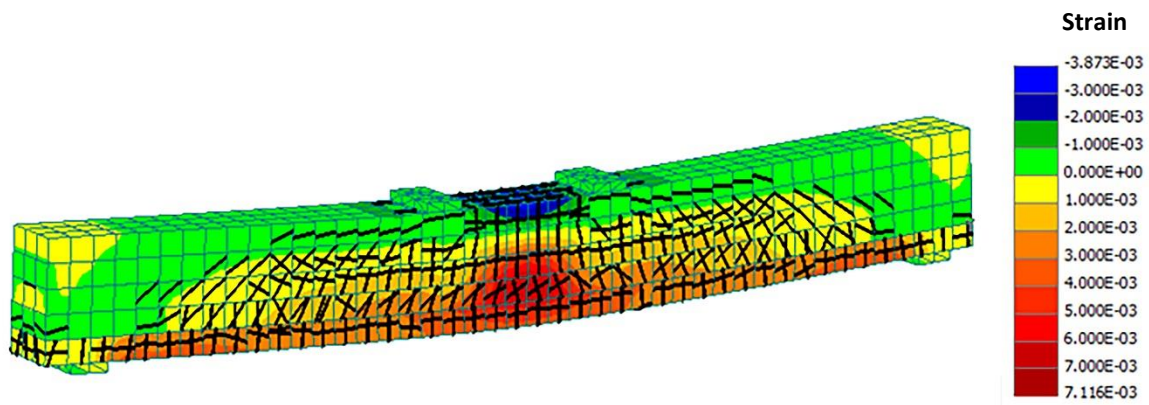
Figure 20 Numerical versus experimental results for the initial beams, the beams strengthened with UHPFRC layers and the beams strengthened UHPFRC layers and steel bars



a



b



c

Figure 21 Crack Pattern at the maximum load for: a) the control beam b) the beam strengthened with UHPFRC layer c) the beam strengthened UHPFRC layers and steel bars

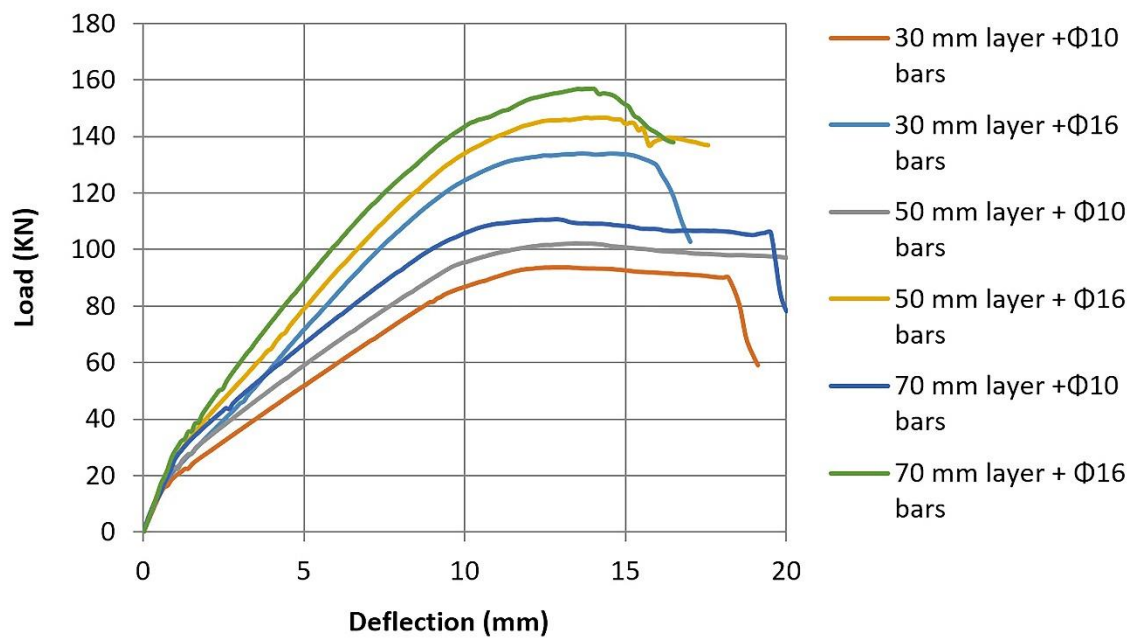


Figure 22 Load versus deflection results for different layer depths and different diameters of the steel bars

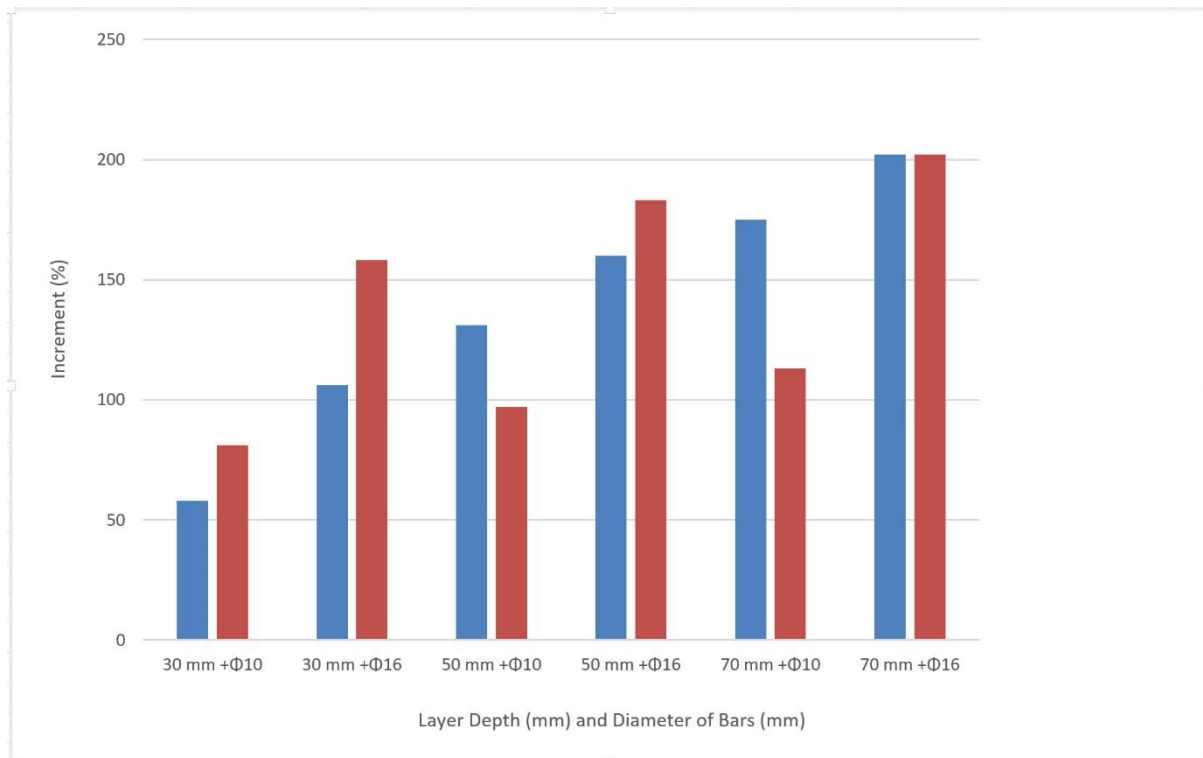


Figure 23 Increment of the yield and the maximum load for the different layer depths and the different diameters of the steel bars